

A graphical framework for proving holographic entanglement entropy inequalities in multipartite systems

Chia-Jui Chou^a, Hans B. Lao^b, Yi Yang^a

^a*Center for Fundamental Physics, School of Physical Science and Technology, ShanghaiTech University, Shanghai, PRC*

^b*Department of Physics, Ateneo de Manila University, Loyola Heights, Quezon City, Philippines*

E-mail: zhoujr@shanghaitech.edu.cn, holao@ateneo.edu, yangyi3@shanghaitech.edu.cn

ABSTRACT: We present a graphical method for proving holographic entanglement entropy inequalities (HEIs) in general multipartite systems. By introducing a geometric representation of the entanglement structure, we develop a systematic approach that enables one to visualize and verify the validity of HEIs for any number of subsystems n . Several theorems are established to formalize this method, and explicit examples are provided for systems with $n = 4$ to 7 entangled regions.

Contents

1	Introduction	1
2	Holographic Entanglement Entropy Inequality	2
2.1	<i>I</i> -basis	3
2.2	HEIs in multipartite systems	4
2.3	Simplex Basis	5
3	Tripartite System	5
3.1	Strong Subadditivity (SSA)	6
3.2	Monogamy of Mutual Information (MMI)	8
4	Multipartite System	10
4.1	Compatible Theorem	10
4.2	Compatible Completely Connected Configuration	13
4.3	Proof of Superbalanced HEIs in CCC Configurations	14
4.4	Joint Form	17
4.5	HEIs in Non-CCC Configurations	20
5	Other Examples	27
6	Conclusion	28

1 Introduction

Entanglement is one of the defining features that distinguishes quantum physics from classical physics, and it can be quantified using the von Neumann entropy. Although calculating entanglement entropy in general quantum field theories is often challenging, Ryu and Takayanagi proposed a geometric prescription based on the AdS/CFT correspondence [1, 2]. According to their proposal, the holographic entanglement entropy (HEE) of a boundary region A is determined by the area of the minimal codimension-2 bulk surface \mathcal{E}_A that is homologous to A :

$$S_A = \min_X \frac{\text{Area}(X)}{4G_N^{(d+2)}}, \quad X = \left\{ \mathcal{E}_A \mid \mathcal{E}_A|_{\partial\mathcal{M}} = \partial A; \exists \mathcal{R}_A \subset \mathcal{M}, \partial\mathcal{R}_A = \mathcal{E}_A \cup A \right\}, \quad (1.1)$$

where \mathcal{E}_A is the Ryu–Takayanagi (RT) surface anchored on ∂A , and \mathcal{R}_A is the corresponding entanglement wedge bounded by \mathcal{E}_A and A . The surface must satisfy a homology constraint, meaning that \mathcal{E}_A can be continuously deformed to A within the bulk region \mathcal{R}_A .

This geometric prescription has allowed one to analyze various properties of entanglement entropy in holographic theories [3–8]. In ordinary quantum systems, the von Neumann entropy obeys several fundamental inequalities, such as subadditivity (SA) [9] and strong subadditivity (SSA) [10], which are central to quantum information theory. However, deriving all such inequalities directly from quantum mechanics is difficult due to the non-commutativity of the reduced density matrices.

In contrast, within holographic theories, many entropy inequalities can be proven geometrically using the RT prescription. These include the proofs of strong subadditivity [11, 12] and monogamy of mutual information (MMI) [12, 13]. Moreover, efforts have been made to classify all possible holographic entropy inequalities systematically, leading to constructions such as the holographic entropy cone [14] and the I_n -theorem for primitive information quantities in multipartite systems [15, 16]. Some of the inequalities derived holographically may not hold for general quantum systems, but they often reveal deeper insights into the geometric and entanglement structure of holographic states. Such states are sometimes called *geometric states* [16–19].

A related development is the proposed correspondence between the entanglement of purification (EoP) and the minimal entanglement wedge cross section (EWCS) [20, 21]. The EoP measures the total correlations between two subsystems A and B , and has been shown to characterize many-body behaviors, such as Z_2 symmetry breaking in the transverse-field Ising model [22, 23].

In our previous work [24], we introduced notations $A_{\langle ij \rangle}$ and $A_{[ij]}$ to describe multipartite systems, allowing one to express entropy inequalities in a balanced form with an equal number of terms on both sides.

In this paper, we extend these ideas by developing a graphical framework to systematically prove holographic entanglement entropy inequalities in multipartite systems. In particular, we establish the *Compatibility Theorem*, *Gapless Theorem*, *Cut Theorem*, and *Configuration Theorem*, which together provide powerful tools for verifying the validity of Holographic Entropy Inequalities (HEIs), irrespective of whether the entangling regions are connected or disconnected.

Section 2 introduces HEIs in multipartite systems, and both the I -basis and the simplex basis are defined. In Section 3, we review the strong subadditivity (SSA) and the monogamy of mutual information (MMI) in the tripartite case. Section 4 presents the main results of this work, outlining a general strategy for proving superbanced HEIs in multipartite systems through the establishment of the four central theorems mentioned above. In Section 5, we illustrate the method with explicit examples of HEIs in 6-partite and 7-partite systems. We conclude in Section 6 with a summary and outlook.

2 Holographic Entanglement Entropy Inequality

The simplest HEI is the subadditivity (SA) in a bipartite system,

$$S_{12} \leq S_1 + S_2. \quad (2.1)$$

For a tripartite system, two fundamental inequalities are known: strong subadditivity (SSA) and monogamy of mutual information (MMI),

$$S_{12} + S_{23} \geq S_{123} + S_2, \quad (2.2)$$

$$S_{12} + S_{23} + S_{13} \geq S_1 + S_2 + S_3 + S_{123}. \quad (2.3)$$

Both can be proven straightforwardly using the Ryu–Takayanagi (RT) prescription.

However, for systems with more than three subsystems, HEIs become far more complicated. In what follows, we develop a systematic approach to prove such inequalities in general multipartite settings.

2.1 I -basis

The inequalities in eqs.(2.1)-(2.3) are written in the so-called S -basis, which directly involve the entropies of the subsystems. In some situations, however, it is more convenient to work with the I -basis, first introduced in [25].

For example, we define the mutual information,

$$I_{12} = S_1 + S_2 - S_{12}, \quad (2.4)$$

and the tripartite information,

$$I_{123} = S_1 + S_2 + S_3 - S_{12} - S_{13} - S_{23} + S_{123}. \quad (2.5)$$

In this notation, SA eq.(2.1) becomes simply $I_{12} \geq 0$, while MMI eq.(2.3) becomes $I_{123} \leq 0$, respectively.

This idea can be generalized to the n -partite information [25],

$$I_{k_1 \dots k_m} = \sum S_{k_\sigma} - \sum S_{k_{\sigma_1} k_{\sigma_2}} + \sum S_{k_{\sigma_1} k_{\sigma_2} k_{\sigma_3}} + \dots + (-1)^{m-1} S_{k_1 \dots k_m} \quad (2.6)$$

or more compactly,

$$I_K = \sum_{J \subseteq K} (-1)^{|J|+1} S_J, \quad (2.7)$$

where K is a set of indices and $|J|$ denotes the number of elements in J .

Note that while $I_{12} \geq 0$ and $I_{123} \leq 0$ have definite signs, higher-order I_K with $|K| > 3$ does not necessarily carry a fixed sign.

Since the RT surface areas diverge near the boundary, an HEI is physically meaningful only if the divergences cancel. This happens when the sets of positive and negative terms share the same indices—such inequalities are called *balanced*. By construction, any n -partite information with $|K| \geq 2$ is balanced. Therefore, any balanced inequality can be expanded in terms of I_K with $|K| \geq 2$:

$$Q_n^b = \sum_{|K| \geq 2} q_K I_K. \quad (2.8)$$

As shown in [26], the fundamental or non-redundant inequalities are in fact superbanced, meaning that they involve only terms with $|K| \geq 3$,

$$Q_n^s = \sum_{|K| \geq 3} q_K I_K. \quad (2.9)$$

For example, both SA eq.(2.1) and MMI eq.(2.3) are balanced, but only MMI is superbanced.

All holographic inequalities can be written as positive combinations of non-redundant HEIs and mutual information I_{ij} . Hence, proving all non-redundant (superbalanced) HEIs is sufficient to establish the entire set of holographic entropy inequalities that define the holographic inequality cone.

The I -basis is particularly convenient for manipulations. A useful identity follows directly from its definition:

$$I_{(K)J} = \sum_{K' \subseteq K} (-1)^{|K'|+1} I_{K'J}, \quad (2.10)$$

where (K) denotes that the subset K is treated as a single region. For example,

$$I_{12(34)} = S_1 + S_2 + S_{34} - S_{12} - S_{134} - S_{234} + S_{1234} = I_{123} + I_{124} - I_{1234} \quad (2.11)$$

In general,

$$I_{(K_1) \dots (K_m)} = \sum_{K'_i \subseteq K_i} (-1)^{\sum_i (|K'_i|+1)} I_{K'_1 \dots K'_m}. \quad (2.12)$$

2.2 HEIs in multipartite systems

In a four-partite system, the independent non-redundant HEIs (up to the permutations of indices) are

$$I_{123} \leq 0, \quad (2.13)$$

$$I_{123} + I_{124} - I_{1234} \leq 0, \quad (2.14)$$

The first is the familiar MMI, and the second can be rewritten as

$$I_{123} + I_{124} - I_{1234} = I_{12(34)} \leq 0, \quad (2.15)$$

which is an enhanced version of MMI. Thus, there are no new inequalities in a four-partite system.

For a five-partite system, however, new independent HEIs appear. Five such non-redundant inequalities can be written as:

$$Q_1^{(5)} = -I_{123} - I_{124} - I_{135} - I_{245} - I_{345} + I_{1234} + I_{1235} + I_{1245} + I_{1345} + I_{2345} - I_{12345}, \quad (2.16)$$

$$Q_2^{(5)} = -I_{123} - I_{124} - I_{125} - I_{345} + I_{1234} + I_{1235} + I_{1245}, \quad (2.17)$$

$$Q_3^{(5)} = -I_{123} - I_{124} - I_{135} - I_{245} + I_{1234} + I_{1235} + I_{1245}, \quad (2.18)$$

$$Q_4^{(5)} = -I_{123} - I_{124} - I_{125} - I_{345} + I_{1235} + I_{1245}, \quad (2.19)$$

$$Q_5^{(5)} = -I_{123} - 2I_{125} - 2I_{134} - I_{145} - I_{234} - I_{235} + 2I_{1234} + 2I_{1235} + I_{1245} + I_{1345} \quad (2.20)$$

These inequalities cannot be expressed simply as combinations of MMI or its enhanced forms. The main goal of this work is to construct a systematic geometric method to prove them.

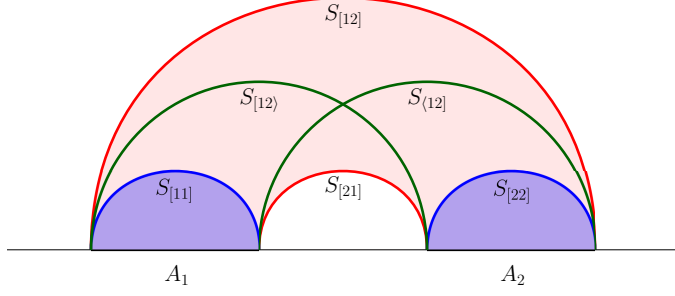


Figure 1. The definition of simplex basis. The six curves are the RT surfaces connecting the ends of entangling regions A_1 and A_2 .

2.3 Simplex Basis

Each entangling region $A_i = [A_i^L, A_i^R]$ is characterized by its left and right endpoints on the boundary. We introduce the simplex basis $S_{[ij]}$, defined as the minimum surface connecting A_i^L and A_j^R in the bulk spacetime.

To illustrate, consider a simple bipartite system. Let $A_{ij} \equiv A_i \cup A_j$ be the union of the two disjoint regions. The entanglement entropy S_{12} can correspond to either a disconnected or a connected configuration of RT surfaces, as shown in Fig.1. For the disconnected case, the total area is $S_{1,2}^d = S_{[11]} + S_{[22]}$, while for the connected case it is $S_{12}^c = S_{[12]} + S_{[21]}$. The physical entropy is the minimum of the two:

$$S_{12} = \min \left(S_{1,2}^d, S_{12}^c \right), \quad (2.21)$$

If $S_{1,2}^d \leq S_{12}^c$, the regions remain disconnected and $S_{12} = S_{1,2}^d = S_1 + S_2$. If $S_{1,2}^d \geq S_{12}^c$, they form a connected configuration and $S_{12} = S_{12}^c \leq S_{1,2}^d = S_1 + S_2$. In either case, the subadditivity inequality eq.(2.1) is automatically satisfied, where equality happens when the two configurations have equal area.

In Fig.1, we also define two auxiliary quantities, $S_{[12\rangle}$ and $S_{\langle 12]}$, which do not appear directly in the final inequalities but are useful as intermediate elements in the graphical proofs.

For a multipartite system, the connected-configuration entropy of a union region $A_{k_1 \dots k_n} = \cup_{i=1}^n A_{k_i}$ can be decomposed as

$$S_{k_1 \dots k_n}^c = \sum_{\sigma=1}^n S_{[k_{\sigma+1} k_{\sigma}]}, \quad (2.22)$$

where $k_1 < k_2 < \dots < k_n$ and $k_{n+1} \equiv k_1$.

The set $\{S_{[ij]}\}$ forms the simplex basis, which will serve as the fundamental building blocks for the graphical analysis of holographic entanglement entropy inequalities in the following sections.

3 Tripartite System

In this section, we consider a system composed of three disjoint entangled regions (A_1, A_2, A_3) satisfying $A_i \cap A_j = \emptyset$. Two fundamental holographic entropy inequalities apply to this system: SSA and MMI.

3.1 Strong Subadditivity (SSA)

For the SSA in eq.(2.2),

$$S_{12} + S_{23} \geq S_{123} + S_2, \quad (3.1)$$

we first examine a configuration where all terms correspond to connected entanglement wedges, which will be called the completely connected (CC) configuration.

In simplex basis, the individual entropies are written as

$$S_2 = S_{[22]}, \quad (3.2)$$

$$S_{12}^c = S_{[12]} + S_{[21]}, \quad (3.3)$$

$$S_{23}^c = S_{[23]} + S_{[32]}, \quad (3.4)$$

$$S_{123}^c = S_{[13]} + S_{[32]} + S_{[21]}. \quad (3.5)$$

Substituting these expressions into eq.(3.1) gives the equivalent inequality

$$S_{[12]} + S_{[23]} \geq S_{[13]} + S_{[22]}. \quad (3.6)$$

To prove eq.(3.6), we compare the two red curves $S_{[12]}$ and $S_{[23]}$ with the blue curves $S_{[13]}$ and $S_{[22]}$ shown schematically in Fig.2(a). We cut the red curves $S_{[12]}$ and $S_{[23]}$ at their intersection point and reconnect them to form two new curves. One of these new curves is homologous to $S_{[22]}$, while the other is homologous to $S_{[13]}$. Since the RT surface minimizes the area within its homology class, each new curve must have an area greater than or equal to the corresponding minimal surface. Hence, the sum of the original red curves is necessarily greater than or equal to that of the blue curves, proving the inequality.

To simplify the visualization, we introduce a circular diagram in Fig.2(b), which encodes the connectivity structure of the RT surfaces. Each entanglement regions A_i is placed along a circle in counterclockwise order, and each RT surface $S_{[ij]}$ is represented as a straight line connecting A_i and A_j . The inequality eq.(3.6) now corresponds to the statement that the sum of the two crossing red lines is greater than the sum of the two blue lines, which we call a cross inequality.

In general, a circular diagram representing an HEI satisfies two properties :

1. The numbers of red and blue lines are equal (ensuring balance).
2. Each node A_i connects to the same number of red and blue lines.

These properties will be useful in later sections to prove more general inequalities.

Having proven SSA in the CC configuration, we now consider the case where some subsystems are disconnected. If S_{12} is disconnected, i.e. $S_{12} = S_{1,2}^d = S_1 + S_2$, the inequality reduces to

$$S_1 + S_{23} \geq S_{123}, \quad (3.7)$$

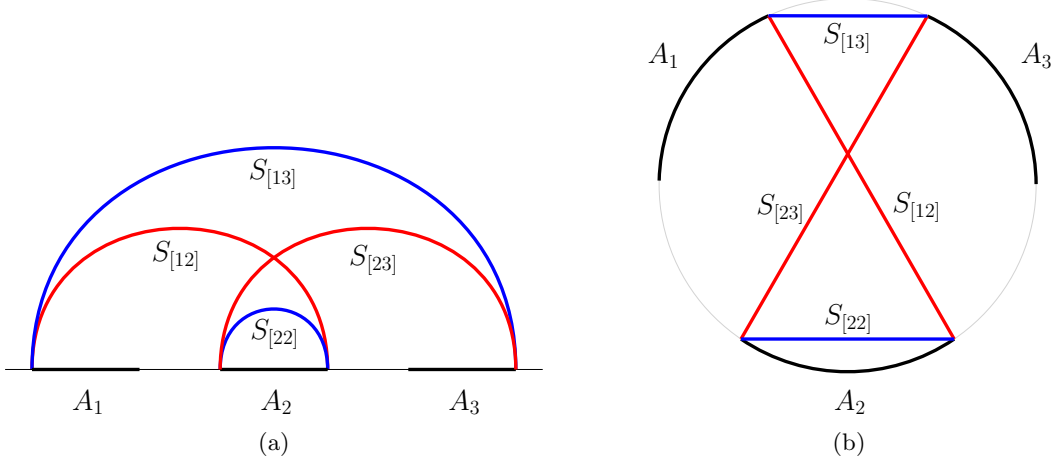


Figure 2. (a) The graphical proof of SSA. (b) Circular diagram of the SSA.

which is simply the SA applied to the composite region A_{23} . The same reasoning applies if S_{13} or S_{23} is disconnected.

If S_{123} is disconnected, four possible configurations arise:

$$S_{1,23}^d = S_1 + S_{23}^c = S_{[11]} + S_{[23]} + S_{[32]}, \quad (3.8)$$

$$S_{12,3}^d = S_{12}^c + S_3 = S_{[12]} + S_{[21]} + S_{[33]}, \quad (3.9)$$

$$S_{2,31}^d = S_2^c + S_{13} = S_{[22]} + S_{[13]} + S_{[31]}, \quad (3.10)$$

$$S_{1,2,3}^d = S_1 + S_2 + S_3 = S_{[11]} + S_{[22]} + S_{[33]}. \quad (3.11)$$

Let us examine these one by one. For the configuration eq.(3.8), the definition of the minimal surface immediately gives

$$S_{123}^c \geq S_1 + S_{23}^c, \quad (3.12)$$

which expands to

$$S_{[13]} + S_{[32]} + S_{[21]} \geq S_{[11]} + S_{[23]} + S_{[32]}, \quad (3.13)$$

or equivalently,

$$S_{[13]} + S_{[21]} \geq S_{[11]} + S_{[23]}. \quad (3.14)$$

Adding this to eq.(3.6) yields

$$S_{[13]} + S_{[21]} + S_{[12]} + S_{[23]} \geq S_{[11]} + S_{[23]} + S_{[13]} + S_{[22]}, \quad (3.15)$$

which simplifies to

$$S_{12}^c = S_{[12]} + S_{[21]} \geq S_{[11]} + S_{[22]} = S_{1,2}^d. \quad (3.16)$$

Hence, the assumption $S_{123} = S_{1,23}^d$ implies $S_{12} = S_{1,2}^d$, and SSA becomes a trivial identity:

$$(S_1 + S_2) + S_{23}^c = (S_1 + S_{23}^c) + S_2. \quad (3.17)$$

Similarly, $S_{123} = S_{12,3}^d$ implies $S_{23} = S_{2,3}^d$, and SSA becomes an identity

$$S_{12}^c + (S_2 + S_3) = (S_{12}^c + S_3) + S_2. \quad (3.18)$$

$S_{123} = S_{2,31}^d$ implies both $S_{12} = S_{1,2}^d$ and $S_{23} = S_{2,3}^d$, and the SSA becomes

$$(S_1 + S_2) + (S_2 + S_3) \geq (S_{13}^c + S_2) + S_2. \quad (3.19)$$

Finally, $S_{123} = S_{1,2,3}^d$ implies both $S_{12} = S_{1,2}^d$ and $S_{23} = S_{2,3}^d$, and the SSA implies a trivial identity

$$(S_1 + S_2) + (S_2 + S_3) = (S_1 + S_2 + S_3) + S_2. \quad (3.20)$$

Thus, SSA eq.(2.2) holds in all possible configurations.

3.2 Monogamy of Mutual Information (MMI)

Next, we turn to the MMI eq.(2.3),

$$S_{12} + S_{13} + S_{23} \geq S_1 + S_2 + S_3 + S_{123}. \quad (3.21)$$

We again begin with the completely connected configuration, in which the inequality can be rewritten in the simplex basis as

$$S_{[12]} + S_{[23]} + S_{[31]} \geq S_{[11]} + S_{[22]} + S_{[33]}. \quad (3.22)$$

To prove eq.(3.22), consider Fig.3(a). The three red lines correspond to the connected RT surfaces $S_{[12]}$, $S_{[23]}$ and $S_{[31]}$; the blue lines represent $S_{[11]}$, $S_{[22]}$ and $S_{[33]}$. Applying the cross inequality to $S_{[12]}$ and $S_{[23]}$,

$$S_{[12]} + S_{[23]} \geq S_{[12]} + S_{[23]}, \quad (3.23)$$

reduces eq.(3.22) to

$$S_{[12]} + S_{[23]} + S_{[31]} \geq S_{[11]} + S_{[22]} + S_{[33]}. \quad (3.24)$$

Now we need to show that the sum of the three red lines is greater than the sum of the three blue lines in Fig.3(b).

Next, applying the cross inequality to $S_{[12]}$ and $S_{[31]}$,

$$S_{[12]} + S_{[31]} \geq S_{[11]} + S_{[23]}, \quad (3.25)$$

yields

$$S_{[23]} + S_{[23]} \geq S_{[22]} + S_{[33]}. \quad (3.26)$$

The final relation, illustrated in Fig.3(c), is another example of the cross inequality between two red and two blue lines. Therefore, the inequality eq.(3.21) is proven in the completely connected configuration.

We call this sequence of operations, i.e., successively eliminating crossed lines by exchanging their endpoints across each gap, the "clean-gap" procedure. It is a key step in all graphical proofs of HEIs.

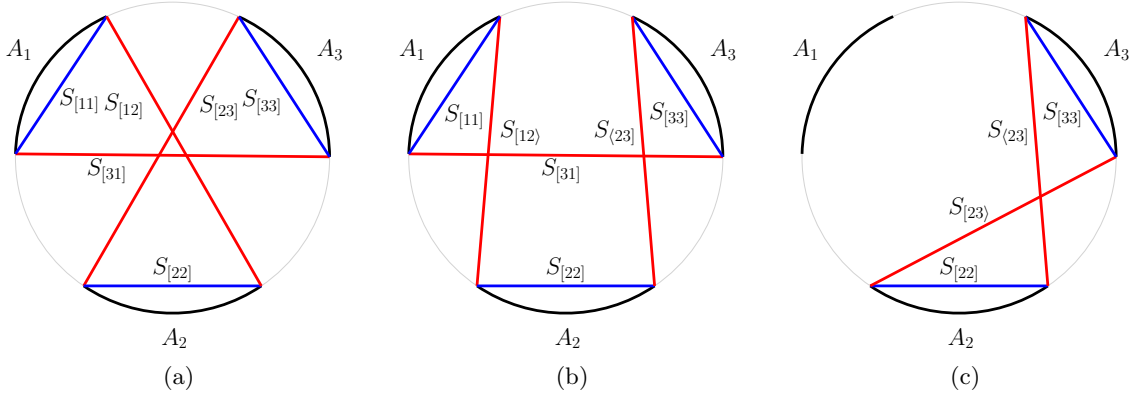


Figure 3. Proof of the MMI through the "clean-gap procedure", shown step by step from (a) to (c) using cross inequalities.

Now consider other configurations. If one of the S_{ij} is disconnected, $S_{ij} = S_{i,j}^d = S_i + S_j$, MMI reduces to SSA. If more than one of them is disconnected, MMI reduce further to SA. On the other hand, if S_{123} is disconnected, the four possible forms in eqs.(3.8-3.11) again apply.

It can be verified that

$$S_{123} = S_{1,23}^d \Rightarrow S_{12} = S_{1,2}^d \text{ and } S_{13} = S_{1,3}^d, \quad (3.27)$$

$$S_{123} = S_{12,3}^d \Rightarrow S_{13} = S_{1,3}^d \text{ and } S_{23} = S_{2,3}^d, \quad (3.28)$$

$$S_{123} = S_{2,31}^d \Rightarrow S_{12} = S_{1,2}^d \text{ and } S_{23} = S_{2,3}^d, \quad (3.29)$$

$$S_{123} = S_{1,2,3}^d \Rightarrow S_{12} = S_{1,2}^d, S_{13} = S_{1,3}^d, \text{ and } S_{23} = S_{2,3}^d. \quad (3.30)$$

In each of the these cases, MMI reduces to a trivial identity, confirming that MMI holds universally.

The examples above illustrate a general strategy for proving holographic entropy inequalities:

1. Express each inequality in the simplex basis under the completely connected configuration.
2. Use successive cross inequalities to prove it graphically.
3. Extend the proof to all other configurations by "cutting" connected terms.

In the third step, we have shown that cutting one surface may require cutting others as well.¹. This observation motivates the Cut Theorem, which will be proved later as a general principle for extending proofs from connected to arbitrary configurations.

¹This is the most important difference between the $(1+1)$ -dimensional CFT and higher dimensional CFT studied in [16, 17, 25, 26]

4 Multipartite System

We now extend our graphical method to general n -partite systems. The approach follows the same logic used for the tripartite case but introduces several new features. In particular, for $n \geq 4$, certain configurations of connected RT surfaces become mutually inconsistent, leading us to define a compatibility condition among entanglement regions.

This section introduces the Compatible Theorem and the concept of Compatible Completely Connected (CCC) configurations, which form the foundation for proving superbalanced holographic entanglement entropy inequalities (HEIs) in higher-partite systems.

4.1 Compatible Theorem

When $n \geq 4$, not all configurations of RT surfaces are physically allowed. To illustrate, consider a 4-partite system. Suppose that both $S_{13} = S_{13}^c$ and $S_{24} = S_{24}^c$ are connected simultaneously. This would imply that

$$S_{13}^c = S_{[13]} + S_{[31]} \leq S_{1,3}^d = S_{[11]} + S_{[33]}, \quad (4.1)$$

$$S_{24}^c = S_{[24]} + S_{[42]} \leq S_{2,4}^d = S_{[22]} + S_{[44]}. \quad (4.2)$$

Adding the two inequalities gives the following result

$$S_{[13]} + S_{[31]} + S_{[24]} + S_{[42]} \leq S_{[11]} + S_{[22]} + S_{[33]} + S_{[44]}, \quad (4.3)$$

i.e. the sum of the red lines (the connected surfaces) is less than the sum of the blue lines (the disconnected surfaces).

However, as we will show, the geometric constraints of the RT prescription imply the opposite inequality:

$$S_{[13]} + S_{[31]} + S_{[24]} + S_{[42]} \geq S_{[11]} + S_{[22]} + S_{[33]} + S_{[44]}. \quad (4.4)$$

This contradiction means that the two surfaces S_{13}^c and S_{24}^c cannot be both connected at the same time; they are incompatible.

To prove eq.(4.4), we employ successive application of the cross inequality, which corresponds to exchanging the endpoints of intersecting red lines in the circular diagram Fig.4.

Then, using the cross inequality,

$$S_{[13]} + S_{[34]} \geq S_{[14]} + S_{[33]}, \quad (4.5)$$

the inequality is reduced to

$$S_{[14]} + S_{[14]} \geq S_{[11]} + S_{[44]}, \quad (4.6)$$

where $S_{[33]}$ cancels out on both sides of the inequality. The circular diagram is shown in Fig.4(d).

Finally, we notice that the inequality eq.(4.11) itself is a cross inequality. Thus, we have verified the inequality eq.(4.4) which is in contradiction to eq.(4.3). We therefore conclude that S_{13} and S_{24} cannot be connected simultaneously. We say that S_{13}^c and S_{24}^c are incompatible.

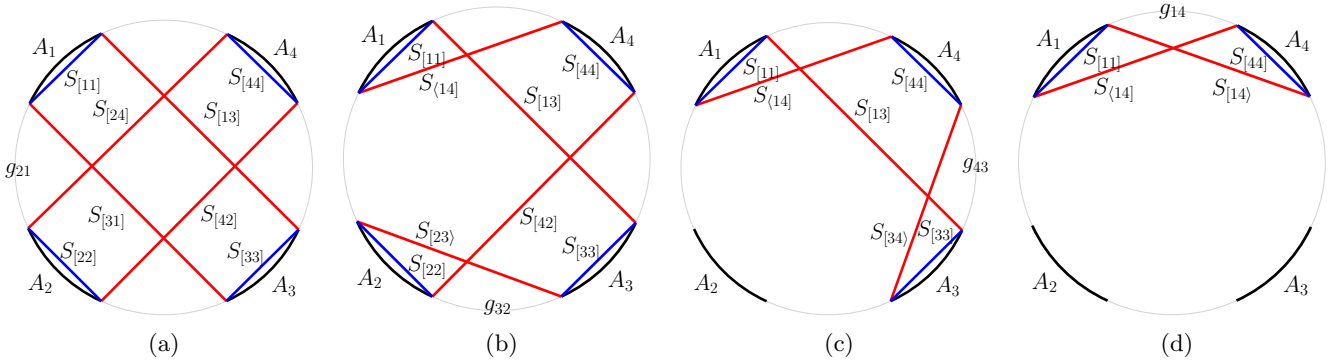


Figure 4. Proving eq.(4.3) by clean-gap procedure.

Let's review how we proved that S_{13}^c and S_{24}^c are incompatible by looking at their circular diagrams step by step:

- First, in Fig.4(a), we observe that the red lines $S_{[31]}$ and $S_{[24]}$ cross each other. Exchanging their endpoints gives two new red lines $S_{[23]}$ and $S_{[14]}$, and the inequality eq.(4.4) reduces to

$$S_{[13]} + S_{[23]} + S_{[14]} + S_{[42]} \geq S_{[11]} + S_{[22]} + S_{[33]} + S_{[44]}. \quad (4.7)$$

This operation (called "skipping the gap g_{21} ") produces a new configuration Fig.4(b) that is smaller according to the cross inequality

$$S_{[31]} + S_{[24]} \geq S_{[23]} + S_{[14]}. \quad (4.8)$$

- Next, in Fig.4(b), the red lines $S_{[23]}$ and $S_{[42]}$ cross each other. Exchanging their endpoints by skipping the gap g_{32} yields $S_{[22]}$ and $S_{[34]}$, and the inequality further reduces to

$$S_{[13]} + S_{[14]} + S_{[34]} \geq S_{[11]} + S_{[33]} + S_{[44]}, \quad (4.9)$$

where term $S_{[22]}$ cancels on both sides. The new configuration Fig.4(c) is smaller according to the cross inequality

$$S_{[23]} + S_{[42]} \geq S_{[22]} + S_{[34]}. \quad (4.10)$$

- Then, in Fig.4(c), the red lines $S_{[13]}$ and $S_{[34]}$ cross each other. Exchanging their endpoints by skipping the gap g_{43} yields $S_{[14]}$ and $S_{[33]}$, and the inequality reduces to

$$S_{[14]} + S_{[14]} \geq S_{[11]} + S_{[44]}, \quad (4.11)$$

where term $S_{[33]}$ cancels on both sides. The new configuration Fig.4(d) is smaller according to the cross inequality

$$S_{[13]} + S_{[34]} \geq S_{[14]} + S_{[33]}. \quad (4.12)$$

- Finally, in Fig.4(d), the pair $S_{[14]}$ and $S_{\langle 14 \rangle}$ cross each other. Exchanging their endpoints by skipping the gap g_{43} yields $S_{[11]}$ and $S_{[44]}$, both of which cancel the original blue lines. This chain of exchanges completes the proof of inequality eq.(4.4), confirming that S_{13}^c and S_{24}^c cannot coexist.

Generally, we have the following Theorem.

Compatible Theorem: In a multipartite system, two connected RT surfaces S_X and $S_{X'}$ are incompatible if the following conditions hold:

1. Complementarity: $X \cap X' = \emptyset$, i.e. the two subsystems do not share boundary regions.
2. Interlaced: the RT surfaces of S_X and $S_{X'}$ are non-planar and cross each other in the circular diagram.

Proof: Arrange X and X' in alternating ordered blocks along the circle,

$$X_1 X'_1 X_2 X'_2 \cdots X_m X'_m \quad (4.13)$$

where $X = X_1 X_2 \cdots X_m$, $X' = X'_1 X'_2 \cdots X'_m$ and m counts the number of alternations.

Assuming both S_X^c and $S_{X'}^c$ are connected, their areas satisfy

$$S_X^c = S_{X_1 \cdots X_m}^c \leq \sum_{k=1}^m S_{X_k}^c, \quad (4.14)$$

$$S_{X'}^c = S_{X'_1 \cdots X'_m}^c \leq \sum_{k=1}^m S_{X'_k}^c. \quad (4.15)$$

Using eq.(2.22), each term expands in the simplex basis as

$$S_X^c = \sum_{k=1}^m \left(S_{[(k+1)_1 k_{n_k}]} + \sum_{\sigma=1}^{n_k-1} S_{[k_{\sigma+1} k_{\sigma}]} \right), \sum_{k=1}^m S_{X_k}^c = \sum_{k=1}^m \sum_{\sigma=1}^{n_k} S_{[k_{\sigma+1} k_{\sigma}]}, \quad (4.16)$$

$$S_{X'}^c = \sum_{k=1}^m \left(S_{[(k'+1)_1 k'_{n_{k'}}]} + \sum_{\sigma=1}^{n'_k-1} S_{[k'_{\sigma+1} k'_{\sigma}]} \right), \sum_{k=1}^m S_{X'_k}^c = \sum_{k'=1}^m \sum_{\sigma=1}^{n'_k} S_{[k'_{\sigma+1} k'_{\sigma}]} \quad (4.17)$$

After canceling common terms, the inequalities eq.(4.14-4.15) reduce to

$$\sum_{k=1}^m S_{[(k+1)_1 k_{n_k}]} \leq \sum_{k=1}^m S_{[k_1 k_{n_k}]} \quad (4.18)$$

$$\sum_{k=1}^m S_{[(k'+1)_1 k'_{n_{k'}}]} \leq \sum_{k=1}^m S_{[k'_1 k'_{n_{k'}}]}. \quad (4.19)$$

Adding the two inequalities gives

$$\sum_{k=1}^m \left(S_{[(k+1)_1 k_{n_k}]} + S_{[(k+1)_1' k'_{n_{k'}}]} \right) \leq \sum_{k=1}^m \left(S_{[k_1 k_{n_k}]} + S_{[k'_1 k'_{n_{k'}}]} \right), \quad (4.20)$$

which means that the sum of the red lines is smaller than the sum of the blue lines in Fig.5.

However, applying the clean-gap procedure reverses the inequality eq.(4.20), leading to a contradiction. Hence, S_X and $S_{X'}$ cannot be connected simultaneously, i.e., S_X^c and $S_{X'}^c$ are incompatible. \square

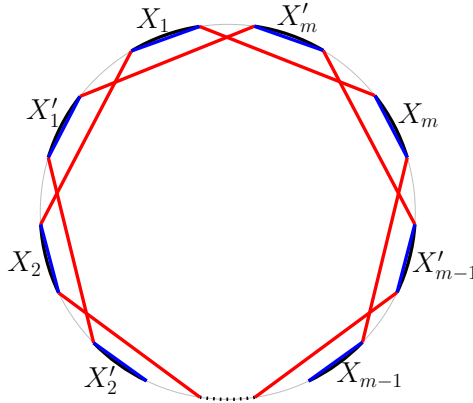


Figure 5. Proof of Compatible Theorem: The sum of the red lines is larger than the sum of the blue lines by the clean-gap procedure, which is in contradiction to eq.(4.20).

	S_{124}	S_{134}	S_{135}	S_{235}	S_{245}
S_{13}					✓
S_{14}				✓	
S_{24}			✓		
S_{25}		✓			
S_{35}	✓				

Table 1. Incompatible pairs are checked in the 5-partite system. One of the RT surfaces in the incompatible pairs must be disconnected.

4.2 Compatible Completely Connected Configuration

The Compatible Theorem imposes strong restrictions for the allowed configurations of a HEI.

In the tripartite case, all terms could be connected simultaneously. However, in a 4-partite system, S_{13}^c and S_{24}^c are incompatible, so at least one of them must be disconnected.

Configurations that satisfy all such compatibility constraints are called Compatible Completely Connected (CCC) configurations. In a 4-partite system, there are two CCC configurations: one with S_{13} disconnected and one with S_{24} disconnected.

In a 5-partite system, compatibility becomes more restrictive. There are five pairs of incompatible RT surfaces as shown in Table 1. At least one surface in each pair must be disconnected.

Accounting for all combinations, there are eleven allowed CCC configurations. Each includes exactly five disconnected terms, either explicitly chosen or implied by others through the constraints demonstrated

earlier. We list all allowed CCC configurations in the following:

$$\text{CCC1} : S_{1,3}^d, S_{1,4}^d, S_{2,4}^d, S_{2,5}^d, S_{3,5}^d \quad (4.21)$$

$$\text{CCC2} : S_{1,3}^d, S_{2,5}^d, S_{12,4}^d \Rightarrow S_{1,4}^d, S_{2,4}^d \quad (4.22)$$

$$\text{CCC3} : S_{2,4}^d, S_{3,5}^d, S_{1,34}^d \Rightarrow S_{1,3}^d, S_{1,4}^d \quad (4.23)$$

$$\text{CCC4} : S_{1,4}^d, S_{2,5}^d, S_{3,51}^d \Rightarrow S_{1,3}^d, S_{3,5}^d \quad (4.24)$$

$$\text{CCC5} : S_{1,3}^d, S_{2,4}^d, S_{23,5}^d \Rightarrow S_{2,5}^d, S_{3,5}^d \quad (4.25)$$

$$\text{CCC6} : S_{1,4}^d, S_{3,5}^d, S_{2,45}^d \Rightarrow S_{2,4}^d, S_{2,5}^d \quad (4.26)$$

$$\text{CCC7} : S_{12,4}^d, S_{1,34}^d \Rightarrow S_{1,3}^d, S_{1,4}^d, S_{2,4}^d \quad (4.27)$$

$$\text{CCC8} : S_{1,34}^d, S_{3,51}^d \Rightarrow S_{1,3}^d, S_{1,4}^d, S_{3,5}^d \quad (4.28)$$

$$\text{CCC9} : S_{3,51}^d, S_{23,5}^d \Rightarrow S_{1,3}^d, S_{3,5}^d, S_{2,5}^d \quad (4.29)$$

$$\text{CCC10} : S_{12,4}^d, S_{2,45}^d \Rightarrow S_{2,4}^d, S_{2,5}^d, S_{1,4}^d \quad (4.30)$$

$$\text{CCC11} : S_{23,5}^d, S_{2,45}^d \Rightarrow S_{2,5}^d, S_{3,5}^d, S_{2,4}^d \quad (4.31)$$

where a certain disconnected term implies that other terms are disconnected. For example, in CCC2, $S_{12,4}^d$ implies $S_{1,4}^d$ and $S_{2,4}^d$ are disconnected.

4.3 Proof of Superbalanced HEIs in CCC Configurations

To prove a HEI in a n -partite system, one must verify it for all possible configurations. However, from our earlier examples, SSA and MMI, we have seen that once an inequality holds in all CCC configuration, it automatically holds in every other configuration. We therefore focus on CCC configurations first.

The first example we consider is a 5-partite HEI in Table 1 of [26],

$$Q_1^{(5)} = -I_{124} - I_{134} - I_{135} - I_{235} - I_{245} + I_{1234} + I_{1235} + I_{1245} + I_{1345} + I_{2345} - I_{12345} \geq 0. \quad (4.32)$$

In the S-basis, this becomes

$$S_{123} + S_{234} + S_{345} + S_{145} + S_{125} \geq S_{12} + S_{23} + S_{34} + S_{45} + S_{15} + S_{12345}. \quad (4.33)$$

Because all terms here are mutually compatible, we can choose every term to be connected in any CCC configuration:

$$S_{123}^c + S_{234}^c + S_{345}^c + S_{145}^c + S_{125}^c \geq S_{12}^c + S_{23}^c + S_{34}^c + S_{45}^c + S_{15}^c + S_{12345}^c. \quad (4.34)$$

Expressing this in the simplex basis gives

$$S_{[13]} + S_{[24]} + S_{[35]} + S_{[41]} + S_{[52]} \geq S_{[12]} + S_{[23]} + S_{[34]} + S_{[45]} + S_{[51]}. \quad (4.35)$$

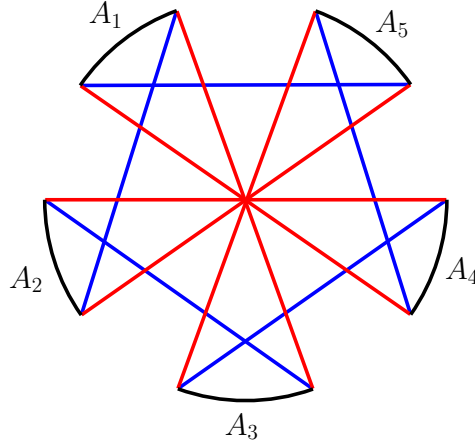


Figure 6. The circular diagram for $Q_1^{(5)}$ in any CCC configuration.

The corresponding circular diagram Fig.6 can be simplified via the clean-gap procedure, showing that the left-hand side is always greater. Thus, $Q_1^{(5)}$ holds in all CCC configurations.

The next example is

$$Q_2^{(5)} = -I_{124} - I_{125} - I_{135} - I_{234} + I_{1234} + I_{1235} + I_{1245} \geq 0, \quad (4.36)$$

which in S-basis reads

$$2S_{123} + S_{124} + S_{125} + S_{134} + S_{145} + S_{235} + S_{245} \geq S_{12} + S_{13} + S_{14} + S_{23} + S_{25} + S_{45} + S_{1234} + S_{1235} + S_{1245}. \quad (4.37)$$

We can now test this inequality under each CCC configuration by expressing all terms in the simplex basis.

1. In the configuration CCC1, eq.(4.37) becomes

$$2S_{[13]} + S_{[14]} + 2S_{[25]} + S_{[31]} + S_{[41]} + S_{[42]} + S_{[52]} \geq 2S_{[11]} + S_{[12]} + S_{[22]} + S_{[23]} + S_{[33]} + S_{[44]} + S_{[45]} + S_{[55]}. \quad (4.38)$$

2. In the configuration CCC2, eq.(4.37) becomes

$$2S_{[13]} + 2S_{[25]} + S_{[31]} + S_{[41]} + S_{[52]} \geq 2S_{[11]} + S_{[22]} + S_{[23]} + S_{[33]} + S_{[45]} + S_{[55]}. \quad (4.39)$$

3. In the configuration CCC3, eq.(4.37) becomes

$$2S_{[13]} + S_{[25]} + S_{[34]} + S_{[41]} + S_{[42]} \geq S_{[11]} + S_{[12]} + S_{[23]} + S_{[33]} + S_{[44]} + S_{[45]}. \quad (4.40)$$

4. In the configuration CCC4, eq.(4.37) becomes

$$2S_{[13]} + S_{[14]} + 2S_{[25]} + S_{[31]} + S_{[41]} + S_{[42]} + S_{[52]} \geq 2S_{[11]} + S_{[12]} + S_{[22]} + S_{[23]} + S_{[33]} + S_{[44]} + S_{[45]} + S_{[55]}, \quad (4.41)$$

which is the same as the first CCC configuration.

5. In the configuration CCC5, eq.(4.37) becomes

$$2S_{[13]} + S_{[25]} + S_{[31]} + S_{[42]} + S_{[52]} \geq S_{[11]} + S_{[12]} + S_{[22]} + S_{[33]} + S_{[45]} + S_{[53]}, \quad (4.42)$$

6. In the configuration CCC6, eq.(4.37) becomes

$$S_{[13]} + S_{[14]} + S_{[25]} + S_{[41]} + S_{[52]} \geq S_{[11]} + S_{[12]} + S_{[23]} + S_{[44]} + S_{[55]}. \quad (4.43)$$

7. In the configuration CCC7, eq.(4.37) becomes

$$2S_{[13]} + S_{[25]} + S_{[34]} + S_{[41]} \geq S_{[11]} + S_{[14]} + S_{[23]} + S_{[33]} + S_{[45]}. \quad (4.44)$$

8. In the configuration CCC8, eq.(4.37) becomes

$$2S_{[13]} + S_{[25]} + S_{[34]} + S_{[41]} + S_{[42]} \geq S_{[11]} + S_{[12]} + S_{[23]} + S_{[33]} + S_{[44]} + S_{[45]}, \quad (4.45)$$

which is the same as the third CCC configuration.

9. In the configuration CCC9, eq.(4.37) becomes

$$2S_{[13]} + S_{[25]} + S_{[31]} + S_{[42]} + S_{[52]} \geq S_{[11]} + S_{[12]} + S_{[22]} + S_{[33]} + S_{[45]} + S_{[53]}, \quad (4.46)$$

which is the same as the fifth CCC configuration.

10. In the configuration CCC10, eq.(4.37) becomes

$$S_{[13]} + S_{[25]} + S_{[41]} + S_{[52]} \geq S_{[11]} + S_{[23]} + S_{[42]} + S_{[55]}. \quad (4.47)$$

11. In the configuration CCC11, eq.(4.37) becomes

$$S_{[13]} + S_{[52]} \geq S_{[12]} + S_{[53]}. \quad (4.48)$$

Although there are eleven CCC configurations, some of them are equivalent, e.g. CCC1 and CCC4 yield the same reduced form.

In each case, the resulting circular diagram (shown in Fig.7) reduces to a positive combination of cross inequalities, confirming that $Q_2^{(5)} \geq 0$ in every CCC configuration.

Let's summarize the strategy we used to prove a HEI in a CCC configuration:

1. Express the HEI in the simplex basis and plot the circular diagrams.
2. Reduce the circular diagrams by the clean-gap procedure.
3. Prove the reduced diagrams by cross inequalities.

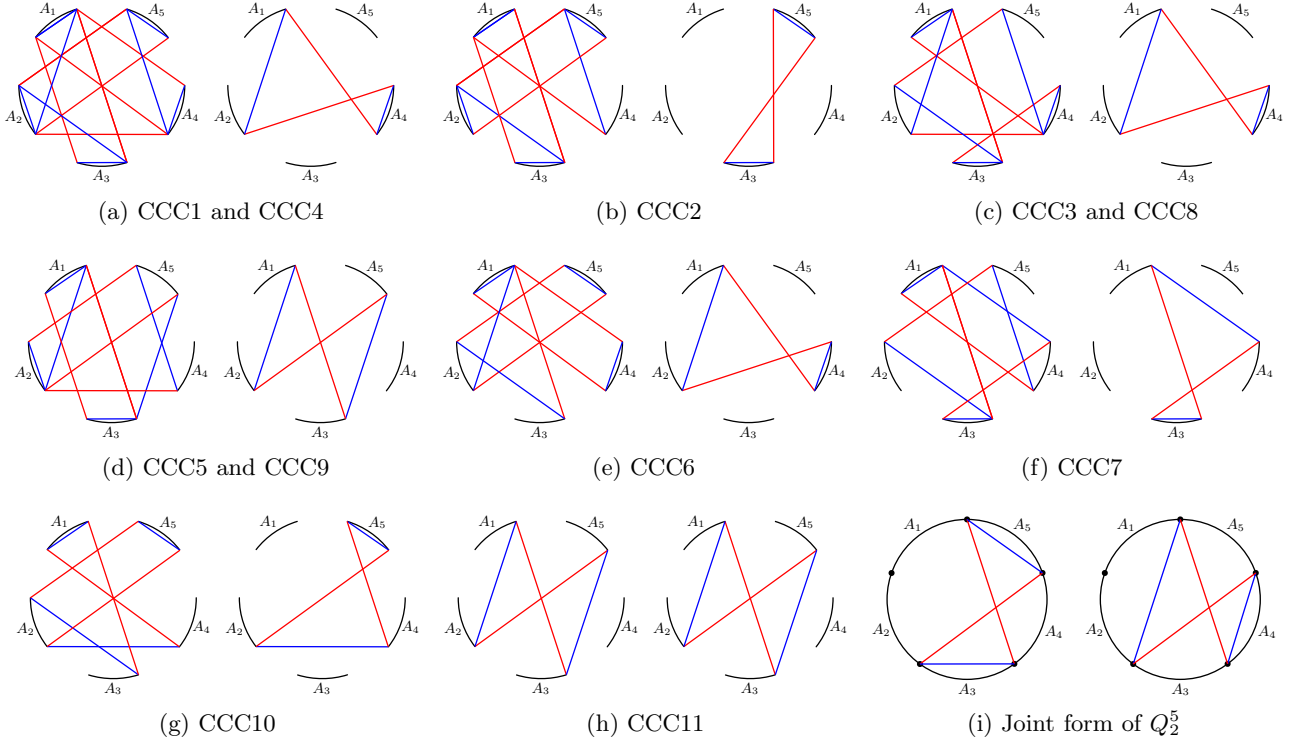


Figure 7. The graphical proof of Q_2^5 in 11 CCC configurations. The joint circular diagram of Q_2^5 is shown in (i).

4.4 Joint Form

The strategy developed in the previous section provides a direct way to prove HEIs in CCC configurations. However, verifying every CCC configuration one by one is often repetitive and inefficient.

To simplify the procedure, we note that the reduced circular diagrams obtained after applying the clean-gap procedure exhibit a common internal structure: the pattern of red and blue lines in each reduced circular diagram is largely independent of the specific region labels A_i . More precisely, if a circular diagram contains no RT surfaces that connect the gaps, i.e. gapless, these gaps can be closed without changing the structure of the inequality. When the adjacent regions A_i are joined in this way, all reduced circular diagrams simplify to just two equivalent joint circular diagrams, as shown in Fig. 7(i).

This motivates us to prove the joint form of a given HEIs, rather than their original form, provided that their circular diagrams are gapless.

There are two important features of the joint form:

1. Complementarity: if \bar{K} is a complement of region K , i.e. $\bar{K} = \{1, \dots, n\} / K$, then the corresponding entropies are equal,

$$S_{\bar{K}} = S_K. \quad (4.49)$$

This identity allows one to simplify a HEI by eliminating one region and replacing its complementary counterpart.

2. Dual representation: any RT surface can be expressed equivalently in two complementary simplex notation, e.g.

$$S_{[ij]} = S_{[j+1,i-1]}. \quad (4.50)$$

This relation becomes particularly useful when gaps between subsystems are closed.

Consider the 5-partite inequality $Q_2^{(5)}$ in eq.(4.37). Because its circular diagram is gapless for all CCC configurations, we can close the gap corresponding to region 5 and remove A_5 using the complementarity relations:

$$S_{25} = S_{134}, S_{45} = S_{123}, S_{125} = S_{34}, S_{145} = S_{23}, \quad (4.51)$$

$$S_{235} = S_{14}, S_{245} = S_{13}, S_{1235} = S_4, S_{1245} = S_3. \quad (4.52)$$

Substituting these identities into eq.(4.37), we obtain the 4-partite joint form:

$$S_{123} + S_{124} + S_{34} \geq S_{12} + S_{1234} + S_3 + S_4, \quad (4.53)$$

which involves only the four regions A_1, A_2, A_3, A_4 .

For the two CCC configurations of the 4-partite system (with either S_{13}^d or S_{24}^d disconnected), eq.(4.53) reduces in the simplex basis to

$$S_{[13]} + S_{[34]} \geq S_{[12]} + S_{[44]}, \quad (4.54)$$

which corresponds to the right-hand diagram in in Fig.7(i). The inequality follows directly from the cross inequality. Hence, the joint form eq.(4.53) is valid, and consequently the original 5-partite inequality $Q_2^{(5)} \geq 0$ is proven.

Now we have an improved strategy to prove a HEI in a CCC configuration:

1. Reduce the HEI to its joint form.
2. Express the the joint form in the simplex basis.
3. Construct the joint circular diagrams and prove the inequality by using cross inequalities.

Before applying this approach to other HEIs, it is useful to recall a general reduction identity in the I-basis,

$$I_{Ki} = I_K + \sum_{Q \subseteq (\bar{K}/i)} (-1)^{|KQ|+1} I_{KQ}, \quad (4.55)$$

which systematically shows how to remove a selected region i for an I-basis.

Applying the improved strategy, one can quickly verify the remaining three HEIs $Q_3^{(5)}$, $Q_4^{(5)}$ and $Q_5^{(5)}$ as follows:

$$Q_3^{(5)} = -I_{125} - I_{135} - I_{145} - I_{234} + I_{1235} + I_{1245} + I_{1345} \geq 0 \quad (4.56)$$

reduces via eq.(4.55) to

$$Q_3^{(5)} = -I_{234} \geq 0, \quad (4.57)$$

which is simply a MMI for the regions A_2, A_3, A_4 .

$$Q_4^{(5)} = -I_{123} - I_{145} - I_{234} - I_{235} + I_{1234} + I_{1235} \geq 0 \quad (4.58)$$

reduces to

$$Q_4^{(5)} = -I_{124} - I_{134} - 2I_{234} + 2I_{1234} \geq 0. \quad (4.59)$$

In the two CCC configurations with S_{13}^d and S_{24}^d disconnected, the inequality becomes

$$S_{13}^d : 2S_{[13]} + S_{[24]} + S_{[34]} \geq S_{[11]} + S_{[12]} + 2S_{[44]}, \quad (4.60)$$

$$S_{24}^d : S_{[13]} + S_{[34]} \geq S_{[12]} + S_{[44]}, \quad (4.61)$$

both of which follow immediately from cross inequalities.

$$Q_5^{(5)} = -I_{123} - 2I_{125} - 2I_{134} - I_{145} - I_{234} - I_{235} + 2I_{1234} + 2I_{1235} + I_{1245} + I_{1345} \geq 0, \quad (4.62)$$

reduces to

$$Q_3^{(5)} = -I_{124} - I_{134} - 2I_{234} + 2I_{1234} \geq 0, \quad (4.63)$$

which is the same as the joint form of the HEI $Q_4^{(5)}$.

In conclusion, proving an HEI through its joint form is considerably simpler than verifying all original CCC configurations individually. The equivalence between the joint and original forms holds whenever the circular diagrams are gapless. This observation leads naturally to the following Gapless Theorem.

Gapless Theorem: a superbalanced HEI in a CCC configuration is always gapless.

Proof: For a n -partite information $I_{k_1 \dots k_n}$ with $n \geq 3$, every connected RT surface

$$S_{k_1 \dots k_i k_{i+1} \dots k_m}^c = \sum_{\sigma=1}^m S_{[k_{\sigma+1} k_{\sigma}]}, \quad (4.64)$$

contributes a term $S_{[k_{i+1} k_i]}$. So, the number of terms $S_{[k_{i+1} k_i]}$ in a completely connected configuration is

$$\sum_{m=0}^{n-1} (-1)^{m+1} C_m^{n-2} = 0. \quad (4.65)$$

On the other hand, to avoid incompatible pairs, we should apply for certain cuts to obtain CCC configurations. However, these cuts do not include ones in the form $C_{j+1,j}^{j,j+1}$ so that the number of terms $S_{[j+1,j]}$ remains zero in the CCC configurations, i.e. a superbalanced HEI in a CCC configuration is always gapless.

□

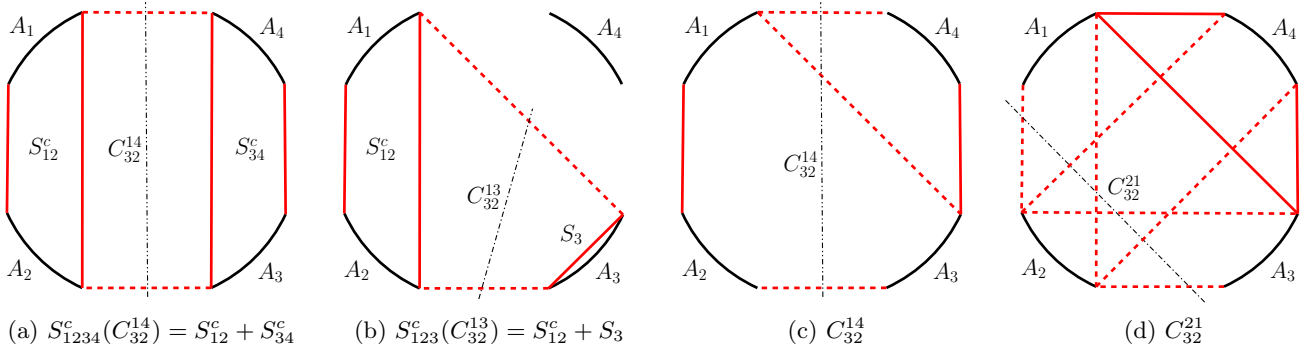


Figure 8. The splits of S_{1234}^c and S_{123}^c

4.5 HEIs in Non-CCC Configurations

We have constructed a systematic method to prove HEIs in the CCC configurations. In this section, we will show that a HEI holding in the CCC configurations ensures that it holds in all other configurations.

Starting from a CCC configuration, we can obtain another configuration by cutting a connected term. Through repeated cuts, all configurations can be obtained. We are going to show that applying a cut will not affect the validity of HEIs.

First, let us formally introduce a concept called a cut C_{kl}^{ij} , which is a segment that intersects with the two RT surfaces $S_{[ij]}$ and $S_{[kl]}$ in a connected HEE. The result of applying a cut C_{kl}^{ij} in a connected HEE is that the pair of lines $S_{[ij]}$ and $S_{[kl]}$ break and rejoin to a new pair of lines, so that the original connected HEE will divide into two connected HEEs by a cut.

We will use the following examples in a 4-partite system to illustrate the effect of a cut as shown in Fig.8. We first consider $S_{1234}^c = S_{[14]} + S_{[43]} + S_{[32]} + S_{[21]}$. In Fig.8(a), we apply a cut C_{32}^{14} that breaks the two dashed lines $S_{[32]}$ and $S_{[14]}$, and rejoins them to the two solid lines $S_{[12]}$ and $S_{[34]}$. The result is that S_{1234}^c splits into two lines $S_{12}^c = S_{[12]} + S_{[21]}$ and $S_{34}^c = S_{[34]} + S_{[43]}$, i.e. $S_{1234}^c(C_{32}^{14}) = S_{12}^c + S_{34}^c$.

Fig.8(b) shows another example of splitting $S_{123}^c = S_{[13]} + S_{[32]} + S_{[21]}$ by applying a cut C_{32}^{13} , which breaks the two dashed lines $S_{[13]}$ and $S_{[32]}$, and rejoins them to the two solid lines $S_{[12]}$ and $S_{[33]}$. Thus S_{123}^c splits into $S_{12}^c = S_{[12]} + S_{[21]}$ and $S_3 = S_{[33]}$, i.e. $S_{123}^c(C_{32}^{13}) = S_{12}^c + S_3$.

In Fig.8(c), we mix the above two examples of S_{1234}^c and S_{123}^c together and apply the cut C_{32}^{14} . We observe that the cut C_{32}^{14} splits not only S_{1234}^c but also S_{123}^c simultaneously, i.e. $S_{1234}^c(C_{32}^{14}) = S_{12}^c + S_{34}^c$ and $S_{123}^c(C_{32}^{14}) = S_{12}^c + S_3$. In addition, we notice that both cuts C_{32}^{13} and C_{32}^{14} split S_{123}^c into $S_{12}^c + S_3$.

Our last example in Fig.8(d) shows that the cut C_{32}^{21} splits $S_{12}^c(C_{32}^{21}) = S_1 + S_2$, $S_{23}^c(C_{32}^{21}) = S_2 + S_3$, $S_{24}^c(C_{32}^{21}) = S_2 + S_4$, $S_{123}^c(C_{32}^{21}) = S_2 + S_{13}^c$, $S_{124}^c(C_{32}^{21}) = S_2 + S_{14}^c$, $S_{234}^c(C_{32}^{21}) = S_2 + S_{34}^c$ and $S_{1234}^c(C_{32}^{21}) = S_2 + S_{134}^c$ simultaneously. In other words, the cut C_{32}^{21} decouples A_2 from the other entanglement regions.

These observations can be summarized into the following Cut Theorem.

Cut Theorem: A cut C_{kj}^{il} splits $S_{i' \dots j' k' \dots l'}^c$ into $S_{i' \dots j'}^c$ and $S_{k' \dots l'}^c$, i.e. $S_{i' \dots j' k' \dots l'}^c(C_{kj}^{il}) = S_{i' \dots j'}^c + S_{k' \dots l'}^c$, if $[i', j'] \subseteq [i, j]$ and $[k', l'] \subseteq [k, l]$, i.e. C_{kj}^{il} induces $C_{k' j'}^{i' l'}$.

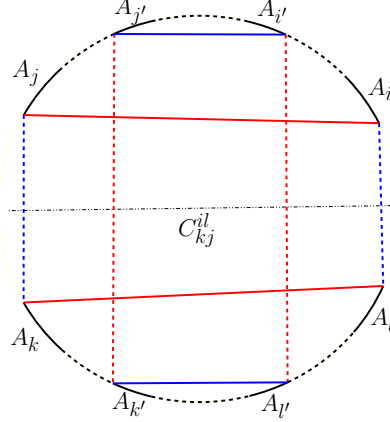


Figure 9. The circular diagram of eq.(4.71).

Proof: By the definition of a cut,

$$S_{i \dots j k \dots l}^c (C_{k j}^{i l}) \rightarrow S_{i \dots j}^c + S_{k \dots l}^c, \quad (4.66)$$

which implies

$$S_{i \dots j k \dots l}^c \geq S_{i \dots j}^c + S_{k \dots l}^c. \quad (4.67)$$

Thus

$$S_{[i l]} + S_{[k j]} + \dots \geq S_{[i j]} + S_{[k l]} + \dots,$$

where \dots on both sides are the same. Then, we have

$$S_{[i l]} + S_{[k j]} - S_{[i j]} - S_{[k l]} \geq 0. \quad (4.68)$$

To show

$$S_{i' \dots j' k' \dots l'}^c (C_{k j}^{i l}) \rightarrow S_{i' \dots j'}^c + S_{k' \dots l'}^c, \quad (4.69)$$

we need to prove

$$S_{[i' l']} + S_{[k' j']} - S_{[i' j']} - S_{[k' l']} \geq 0. \quad (4.70)$$

It is sufficient to show that

$$S_{[i' l']} + S_{[k' j']} - S_{[i' j']} - S_{[k' l']} \geq S_{[i l]} + S_{[k j]} - S_{[i j]} - S_{[k l]}$$

or

$$S_{[i' l']} + S_{[k' j']} + S_{[i j]} + S_{[k l]} \geq S_{[i l]} + S_{[k j]} + S_{[i' j']} + S_{[k' l']}. \quad (4.71)$$

Therefore, we need to show that the sum of the red lines is greater than the sum of the blue lines illustrated in Fig.9, which can be verified by using the clean-gap procedure. This completes the proof of the Cut Theorem. \square

We have shown that a connected RT surface can be split into two connected ones by applying a cut. This step can be performed repeatedly from a HEI in a CCC configuration. All possible configurations can be obtained by applying a finite number of cuts.

For a n -partite system, there are at most $\frac{n(n+1)}{2}$ lines in a CCC configuration. For a line $[ij]$, there are $\sum_{k=1}^{j-i} k$ dual segments to form non-intersected pairs. Thus, there are in total

$$N_n = \frac{n}{2} \sum_{m=1}^{n-1} \sum_{k=1}^m k = \frac{n^2(n^2-1)}{12} \quad (4.72)$$

non-intersected pairs, and each pair is associated to a cut.

Among all the cuts, some cuts will induce other ones. We therefore classify the cuts into $(n-1)$ levels for a n -partite system. There are $\frac{nk(n-k)}{2}$ cuts in the k -level and each of them induces $(k-1)$ -level cuts and therefore the lower level cuts.

- at level $k = 1$, there are $\frac{n(n-1)}{2}$ lowest cuts C_{ji}^{ij} : a cut that does not induce any other cut.
- at level $k = n-1$, there are $\frac{n(n-1)}{2}$ highest cuts: a cut that completely divides the circular diagram into two independent parts.

Let's list the cuts for some lower n -partite systems.

- For a tripartite system, there are in total $N_3 = \frac{3^2(3^2-1)}{12} = 6$ cuts. They are 3 level 1 (lowest) cuts and 3 level 2 (highest) cuts which induce the level 1 cuts as shown in Fig.10(a).
- For a 4-partite system, there are in total $N_4 = \frac{4^2(4^2-1)}{12} = 20$ cuts. They are 6 level 1 (lowest) cuts, 8 level 2 cuts and 6 level 3 (highest) cuts as shown in Fig.10(b).
- For a 5-partite system, there are in total $N_5 = \frac{5^2(5^2-1)}{12} = 50$ cuts. They are 10 level 1 (lowest) cuts, 15 level 2 cuts, 15 level 3 cuts and 10 level 6 (highest) cuts as shown in Fig.10(c).

Since applying any combination of cuts on a CCC configuration leads to a new configuration, naively, we need to consider in total 2^{N_n} configurations for a n -partite system. This number grows rapidly with the number of entanglement regions n and it is usually impossible to check them one by one. However, since higher level cuts induce lower level cuts, many of the naive configurations are not allowed.

To count the number of allowed configurations, we realize that the cuts form a Dependency Acyclic Graph (DAG) for any n -partite system. We can use dynamical programming methods to count the independent paths of a DAG, and each independent path is associated with an allowed configuration.

For a tripartite system, there are naively $2^6 = 64$ configurations. Among them, 17 configurations are allowed. For a 4-partite system, there are naively $2^{20} = 1048576$ configurations with 1570 of them being allowed (after considering compatibility). For a 5-partite system, there are naively $2^{50} = 1125899906842624$ configurations with 2864048 of them being allowed (after considering compatibility).

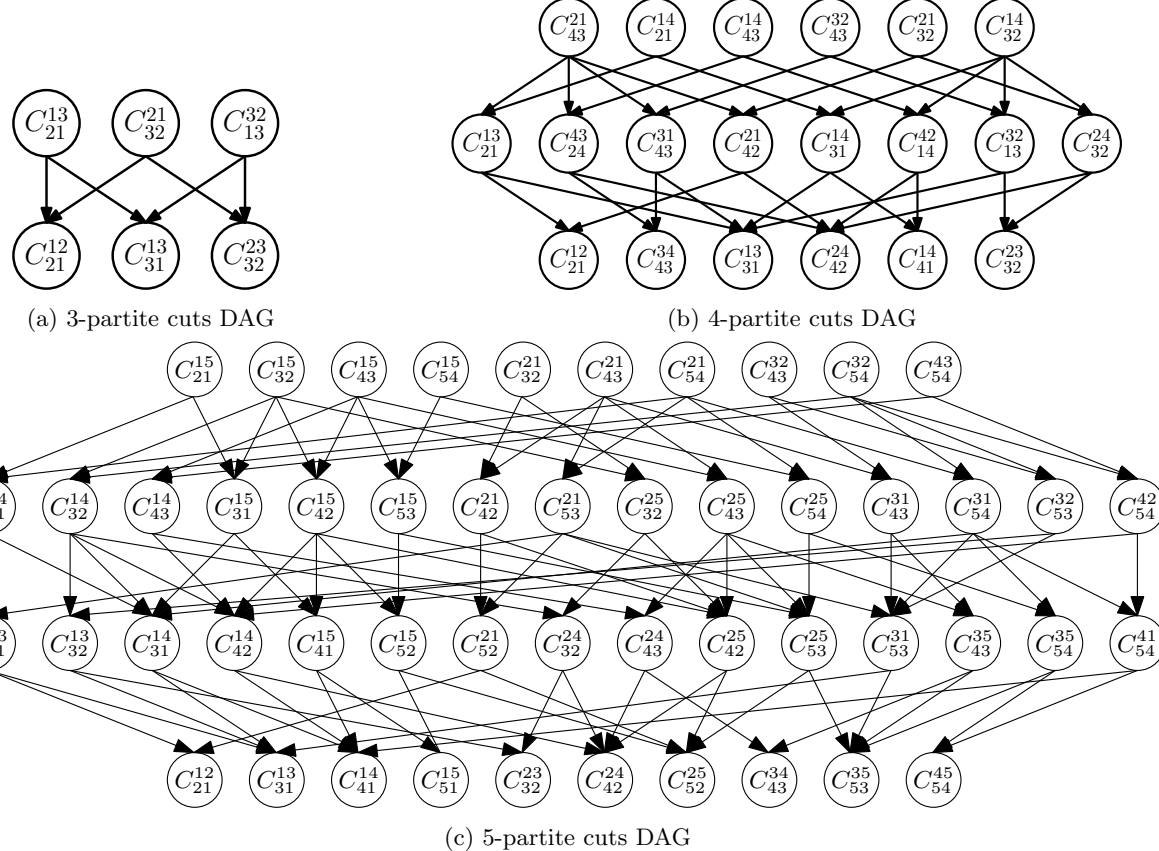


Figure 10. The Dependency Acyclic Graph (DAG) for cuts.

We see that the number of allowed configurations is much less than the number of naive configurations. Nevertheless, checking all allowed configurations one by one is still a tedious job. Remarkably, we can prove that if a HEI holds in CCC configurations, then it holds in any other configurations.

Configuration Theorem. If a balanced HEI is valid in CCC configurations, then it is valid in all configurations.

Proof. Any configuration can be obtained from a CCC configuration by a sequence of cuts. In addition, a superbalanced HEI can be reduced to a balanced HEI by applying a cut. Therefore, by mathematical induction, it suffices to prove the following statement:

If a balanced HEI is valid in a configuration C , which is not necessarily a CCC configuration, then the reduced HEI obtained by applying a cut is also valid in the same configuration C with that cut.

However, it is straightforward to show that the reduced HEI in simplex basis has the same form for the original configuration C with or without the cut. Consequently, we are free to prove the validity of the reduced HEI either in the configuration C or in the configuration C with the cut. This is the key observation used to establish the Configuration Theorem.

1. Assume that a balanced HEI

$$Q_n^b = \sum_{|K| \geq 2} q_K I_K \geq 0, \quad (4.73)$$

is valid in a configuration C .

2. Apply a cut C_{kj}^{il} to this HEI. The reduced HEI is

$$Q_n^b(C_{kj}^{il}) = \sum_{|K| \geq 2} q_K I_K(C_{kj}^{il}), \quad (4.74)$$

where the action of the cut C_{kj}^{il} on the I -basis can be calculated as

$$I_K(C_{kj}^{il}) = I_K + \sum_{\substack{I \subseteq K \cap [i,j] \\ J \subseteq K \cap [k,l]}} (-1)^{|IJ|+1} I_{(I)(J)}. \quad (4.75)$$

Therefore,

$$\begin{aligned} Q_n^b(C_{kj}^{il}) &= \sum_{|K| \geq 2} q_K I_K + \sum_{|K| \geq 2} q_K \sum_{\substack{I \subseteq K \cap [i,j] \\ J \subseteq K \cap [k,l]}} (-1)^{|IJ|+1} I_{(I)(J)} \\ &= Q_n^b + \sum_{\substack{I \subseteq [i,j] \\ J \subseteq [k,l]}} \left[(-1)^{|IJ|+1} \sum_{K' \subseteq [i,j] \cup [k,l]} q_{IJK'} \right] I_{(I)(J)} \\ &= Q_n^b + \sum_{\substack{I \subseteq [i,j] \\ J \subseteq [k,l]}} q'_{IJ} I_{(I)(J)}, \end{aligned} \quad (4.76)$$

where

$$q'_{IJ} = (-1)^{|IJ|+1} \sum_{K' \subseteq [i,j] \cup [k,l]} q_{IJK'}. \quad (4.77)$$

Now consider evaluating the reduced HEI $Q_n^b(C_{kj}^{il})$ in the configuration C with or without the cut C_{kj}^{il} . By assumption, the first term in eq.(4.76), Q_n^b , is strictly greater than 0 in the configuration C . For the remaining terms, we distinguish two cases:

(a) For those terms whose coefficients satisfy $q'_{IJ} \geq 0$, we choose to evaluate them in the configuration C without the cut C_{kj}^{il} . In this case, we have $S_I + S_J \geq S_{IJ}^c$, which implies

$$I_{(I)(J)} = S_I + S_J - S_{IJ}^c \geq 0, \quad (4.78)$$

and hence $q'_{IJ} I_{(I)(J)} \geq 0$. Therefore, the sum of the two nonnegative quantities is nonnegative:

$$Q_n^b + q'_{IJ} I_{(I)(J)} \geq 0. \quad (4.79)$$

(b) For those terms whose coefficients satisfy $q'_{IJ} \leq 0$, we choose to evaluate them in the configuration C with the cut C_{kj}^{il} . In that configuration, we have $S_I + S_J \leq S_{IJ}^c$, which implies

$$I_{(I)(J)} = S_I + S_J - S_{IJ}^c \leq 0, \quad (4.80)$$

and thus again $q'_{IJ} I_{(I)(J)} \geq 0$. Consequently, the sum of the two nonnegative quantities is nonnegative:

$$Q_n^b + q'_{IJ} I_{(I)(J)} \left(C_{kj}^{il} \right) \geq 0. \quad (4.81)$$

This completes the proof of the Configuration Theorem. \square

The arguments in the above proof are quite formal. In this subsection, we illustrate the Configuration Theorem with a concrete example. Consider the superbalanced HEI in a 4-partite system

$$Q = -I_{123} - I_{124} + I_{1234} \geq 0. \quad (4.82)$$

In a 4-partite system, there are two CCC configurations, $\{S_{1,3}^d\}$ and $\{S_{2,4}^d\}$. Since these two CCC configurations are related by a symmetry, it suffices to consider only one of them, say $\{S_{1,3}^d\}$. Expressing the HEI in eq.(4.82) in simplex basis of this CCC configuration, we obtain

$$Q = -S_{[1,1]} + S_{[1,2]} - S_{[2,2]} + S_{[2,4]} + S_{[3,1]} - S_{[3,4]}, \quad (4.83)$$

whose circular diagram is shown in Fig.11(a). It is straightforward to verify that $Q > 0$ by using cross inequalities.

Next, we apply a cut C_{21}^{12} to Q :

$$Q(C_{21}^{12}) = -I_{123} - I_{124} + I_{1234} + I_{12} = Q + I_{12}, \quad (4.84)$$

which, in simplex basis becomes

$$Q(C_{21}^{12}) = -S_{[2,1]} + S_{[2,4]} + S_{[3,1]} - S_{[3,4]}, \quad (4.85)$$

and its circular diagram is plotted in Fig.11(b). As in the case of Q , it is straightforward to show that $Q(C_{21}^{12}) > 0$ by a cross inequality.

Now consider applying a different cut, C_{43}^{34} , to Q :

$$Q(C_{43}^{34}) = -I_{123} - I_{124} + I_{1234} - I_{34} = Q - I_{34}. \quad (4.86)$$

In this case, the coefficient of I_{34} is negative.

In the simplex basis, eq.(4.86) becomes

$$Q(C_{43}^{34}) = -S_{[1,1]} + S_{[1,2]} - S_{[2,2]} + S_{[2,4]} + S_{[3,1]} - S_{[3,3]} + S_{[4,3]} - S_{[4,4]}, \quad (4.87)$$

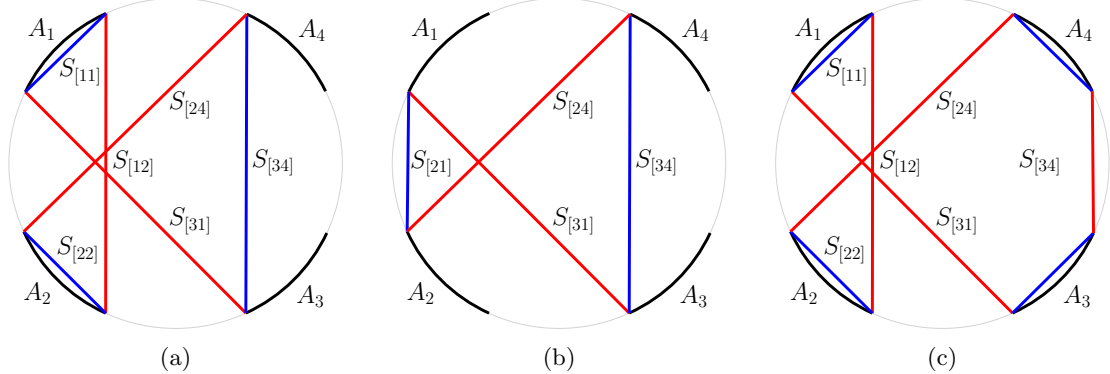


Figure 11. (a) Circular diagram corresponding to eq.(4.83). (b) Circular diagram corresponding to eq.(4.85). (c) Circular diagram corresponding to eq.(4.87).

whose circular diagram is plotted in Fig.11(c). As expected, it is not possible to show that $Q(C_{43}^{34}) > 0$ using only cross inequalities. To establish its positivity, we must use the additional information that C_{43}^{34} cuts $S_{34} = S_3 + S_4$, i.e.

$$S_{34}^c \geq S_3 + S_4, \quad (4.88)$$

which implies

$$S_{[3,4]} + S_{[4,3]} \geq S_{[3,3]} + S_{[4,4]}. \quad (4.89)$$

Therefore,

$$Q(C_{43}^{34}) \geq -S_{[1,1]} + S_{[1,2]} - S_{[2,2]} + S_{[2,4]} + S_{[3,1]} - S_{[3,4]}, \quad (4.90)$$

which is exactly the same expression as in eq.(4.83). Since eq.(4.83) has already been shown to be strictly positive, we conclude that

$$Q(C_{43}^{34}) \geq 0 \quad (4.91)$$

holds conditionally, due to the constraint imposed by the cut C_{43}^{34} .

We have thus shown that a balanced HEI which is valid in certain configurations remains (conditionally) valid after applying a cut. We are now ready to present a complete strategy for proving a superbalanced HEI:

1. Obtain the joint form of the superbalanced HEI.
2. Express this joint form in CCC configurations using the simplex basis.
3. Plot the corresponding joint circular diagram and prove its validity by cross inequalities.
4. Conclude that the HEI is valid in all configurations, by the Configuration Theorem.

5 Other Examples

In this section, we present further examples for $n = 6$ and 7.

In [27], a family of HEIs in the 6-partite system was discovered. We will prove two of them using our strategy as illustrative examples. Using the notation of [27], the two HEEs we consider are

$$Q_{\{4,3\}}^{[24]} = -I_{123} - I_{126} - I_{156} - I_{246} + I_{1236} + I_{1246} + I_{1256}, \quad (5.1)$$

$$Q_{\{5,3\}}^{[13]} = -I_{123} - I_{125} - I_{126} - I_{356} - I_{456} + I_{1236} + I_{1256} + I_{3456}. \quad (5.2)$$

By eliminating the region A_6 , the above two HEIs reduce to their joint forms

$$Q_{\{4,3\}}^{[24]} = -I_{135} - I_{145} - I_{234} - I_{245} + I_{1245} + I_{1345} + I_{2345}, \quad (5.3)$$

$$Q_{\{5,3\}}^{[13]} = -I_{124} - I_{135} - I_{145} - I_{235} - I_{245} + I_{1245} + I_{1345} + I_{2345}, \quad (5.4)$$

which is effectively a HEI in a 5-partite system. We now study these joint forms in the 11 CCC configurations for $n = 5$.

For $Q_{\{4,3\}}^{[24]}$, in 11 CCC configurations we obtain

$$\text{CCC1, 4} : 2S_{[14]} + S_{[23]} + S_{[25]} + 2S_{[35]} \geq S_{[11]} + S_{[12]} + S_{[22]} + S_{[45]} + 2S_{[55]} \quad (5.5)$$

$$\text{CCC2} : S_{[14]} + S_{[23]} + S_{[25]} + S_{[35]} \geq S_{[11]} + S_{[22]} + S_{[45]} + S_{[55]} \quad (5.6)$$

$$\text{CCC3, 5, 8, 9} : S_{[14]} + S_{[23]} + 2S_{[35]} \geq S_{[12]} + S_{[22]} + S_{[45]} + S_{[55]} \quad (5.7)$$

$$\text{CCC6} : 2S_{[14]} + S_{[23]} + 2S_{[35]} \geq S_{[11]} + S_{[12]} + S_{[33]} + 2S_{[55]} \quad (5.8)$$

$$\text{CCC7} : S_{[23]} + S_{[35]} \geq S_{[22]} + S_{[45]} \quad (5.9)$$

$$\text{CCC10} : S_{[14]} + S_{[23]} + S_{[35]} \geq S_{[11]} + S_{[33]} + S_{[55]} \quad (5.10)$$

$$\text{CCC11} : S_{[14]} + S_{[23]} + 2S_{[35]} \geq S_{[12]} + S_{[25]} + S_{[33]} + S_{[55]} \quad (5.11)$$

each of which can be verified straightforwardly by cross inequalities.

For $Q_{\{5,3\}}^{[13]}$, in 11 CCC configurations we obtain,

$$\text{CCC1, 2, 4, 5, 9} : S_{[14]} + S_{[24]} + 2S_{[35]} + S_{[41]} + S_{[52]} \geq S_{[11]} + S_{[22]} + 2S_{[34]} + S_{[45]} + S_{[55]} \quad (5.12)$$

$$\text{CCC3, 7, 8} : S_{[24]} + 2S_{[35]} + S_{[41]} + S_{[52]} \geq S_{[22]} + S_{[31]} + S_{[34]} + S_{[45]} + S_{[55]} \quad (5.13)$$

$$\text{CCC6, 10, 11} : S_{[14]} + S_{[24]} + 2S_{[35]} + S_{[41]} + S_{[52]} \geq S_{[11]} + S_{[25]} + 2S_{[34]} + S_{[42]} + S_{[55]} \quad (5.14)$$

which again can be proved directly by cross inequalities.

Finally, we turn to the 7-partite system. In [27], the following HEI in 7-partite system was discovered,

$$\begin{aligned}
& S_{1245} + S_{1246} + S_{1257} + S_{1456} + S_{1457} + S_{1345} + S_{1346} \\
& + S_{1357} + S_{2456} + S_{2457} + S_{2345} + S_{2346} + S_{2357} + S_{3456} + S_{3457} \\
& \geq S_{123} + S_{145} + S_{146} + S_{157} + S_{245} + S_{246} + S_{257} + S_{345} \\
& + S_{346} + S_{357} + S_{12456} + S_{12457} + S_{13456} + S_{13457} + S_{23456} + S_{23457}, \tag{5.15}
\end{aligned}$$

which can be written in the superbalanced form using I-basis as

$$\begin{aligned}
Q_7 = & -I_{123} - I_{145} - I_{147} - I_{156} - I_{245} - I_{247} - I_{256} - I_{345} - I_{347} - I_{356} \\
& + I_{1245} + I_{1247} + I_{1256} + I_{1345} + I_{1347} + I_{1356} + I_{1456} + I_{1457} \\
& + I_{2345} + I_{2347} + I_{2356} + I_{2456} + I_{2457} + I_{3456} + I_{3457} \\
& - I_{12456} - I_{12457} - I_{13456} - I_{13457} - I_{23456} - I_{23457}, \tag{5.16}
\end{aligned}$$

which is effectively a HEI in a 5-partite system.

By eliminating the region A_5 , this HEI reduces to its joint form,

$$Q_7 = -I_{123} - I_{167} - I_{267} - I_{367} + I_{1267} + I_{1367} + I_{2367}. \tag{5.17}$$

By applying the permutation $(1, 2, 3, 6, 7) \rightarrow (2, 3, 4, 1, 5)$, we can map the HEI Q_7 in eq.(5.17) to $Q_3^{(5)}$ in eq.(4.59), which has already been proved.

6 Conclusion

In this paper, we have developed a systematic strategy to prove Holographic Entropy Inequalities (HEIs) in multipartite systems. This strategy integrates several key conceptual and methodological ingredients.

First, we introduced the simplex basis. Any HEI in a fixed configuration can be expressed in this basis and represented graphically by a circular diagram. We analyzed the potential incompatibility between two connected RT surfaces and established the Compatibility Theorem, which led to the definition of Compatible Completely Connected (CCC) configurations. We showed that the circular diagram corresponding to a superbalanced HEI in a CCC configuration is gapless and can be systematically simplified using the clean-gap procedure. The resulting reduced diagram can then be directly verified by cross inequalities.

Moreover, we demonstrated that the gapless structure of an HEI in a CCC configuration allows it to be reduced to a joint form, which greatly simplifies its verification.

To extend the analysis beyond CCC configurations, we introduced the critical notion of a cut. By successively applying cuts to an HEI starting from a CCC configuration, one can systematically explore all possible configurations. In an n -partite system, there are in total $\frac{n^2(n^2-1)}{12}$ cuts, organized into $(n-1)$ hierarchical levels. We proved the Cut Theorem, which shows that cuts at higher levels induce cuts at lower levels, thereby defining a dependency acyclic graph (DAG) structure among the cuts.

Finally, we established the Configuration Theorem, which states that if an HEI holds in all CCC configurations, then it necessarily holds in every configuration.

We applied our strategy to rigorously prove several example HEIs for systems with $n = 3, 4, 5, 6$, and 7 parties. Having a systematic verification framework in place opens the door to a systematic construction of new HEIs in multipartite systems. At present, HEIs are fully understood only for $n = 3, 4, 5$ and partially for $n = 6, 7$. Constructing general HEIs for higher-partite systems remains an extremely challenging problem. We plan to address the systematic construction of general HEIs in multipartite systems in future work.

References

- [1] Shinsei Ryu and Tadashi Takayanagi. Holographic derivation of entanglement entropy from AdS/CFT. *Phys. Rev. Lett.*, 96:181602, 2006.
- [2] Igor R. Klebanov, David Kutasov, and Arvind Murugan. Entanglement as a probe of confinement. *Nuclear Physics B*, 796(1):274–293, 2008.
- [3] Dmitri V. Fursaev. Proof of the holographic formula for entanglement entropy. *JHEP*, 09:018, 2006.
- [4] Veronika E. Hubeny, Mukund Rangamani, and Tadashi Takayanagi. A Covariant holographic entanglement entropy proposal. *JHEP*, 07:062, 2007.
- [5] Matthew Headrick. Entanglement Renyi entropies in holographic theories. *Phys. Rev. D*, 82:126010, 2010.
- [6] Horacio Casini, Marina Huerta, and Robert C. Myers. Towards a derivation of holographic entanglement entropy. *JHEP*, 05:036, 2011.
- [7] Aitor Lewkowycz and Juan Maldacena. Generalized gravitational entropy. *JHEP*, 08:090, 2013.
- [8] Mukund Rangamani and Tadashi Takayanagi. *Holographic Entanglement Entropy*. Springer International Publishing, 2016.
- [9] Huzihiro Araki and Elliot H. Lieb. Entropy inequalities. *Communications in Mathematical Physics*, 18(2):160–170, 1970.
- [10] Elliott H. Lieb and Mary Beth Ruskai. Some operator inequalities of the schwarz type. *Advances in Mathematics*, 12(2):269–273, 1974.
- [11] Matthew Headrick and Tadashi Takayanagi. A Holographic proof of the strong subadditivity of entanglement entropy. *Phys. Rev. D*, 76:106013, 2007.
- [12] Aron C. Wall. Maximin Surfaces, and the Strong Subadditivity of the Covariant Holographic Entanglement Entropy. *Class. Quant. Grav.*, 31(22):225007, 2014.
- [13] Patrick Hayden, Matthew Headrick, and Alexander Maloney. Holographic Mutual Information is Monogamous. *Phys. Rev. D*, 87(4):046003, 2013.
- [14] Ning Bao, Sepehr Nezami, Hirosi Ooguri, Bogdan Stoica, James Sully, and Michael Walter. The Holographic Entropy Cone. *JHEP*, 09:130, 2015.
- [15] Michael Walter, David Gross, and Jens Eisert. Multi-partite entanglement. 12 2016.

- [16] Veronika E. Hubeny, Mukund Rangamani, and Massimiliano Rota. Holographic entropy relations. *Fortsch. Phys.*, 66(11-12):1800067, 2018.
- [17] Temple He, Matthew Headrick, and Veronika E. Hubeny. Holographic Entropy Relations Repackaged. *JHEP*, 10:118, 2019.
- [18] Wu-zhong Guo. Correlations in geometric states. *JHEP*, 08:125, 2020.
- [19] Wu-zhong Guo. Entanglement spectrum of geometric states. *JHEP*, 02:085, 2021.
- [20] Tadashi Takayanagi and Koji Umemoto. Entanglement of purification through holographic duality. *Nature Phys.*, 14(6):573–577, 2018.
- [21] Phuc Nguyen, Trithep Devakul, Matthew G. Halbasch, Michael P. Zaletel, and Brian Swingle. Entanglement of purification: from spin chains to holography. *JHEP*, 01:098, 2018.
- [22] Arpan Bhattacharyya, Tadashi Takayanagi, and Koji Umemoto. Entanglement of Purification in Free Scalar Field Theories. *JHEP*, 04:132, 2018.
- [23] Arpan Bhattacharyya, Alexander Jahn, Tadashi Takayanagi, and Koji Umemoto. Entanglement of Purification in Many Body Systems and Symmetry Breaking. *Phys. Rev. Lett.*, 122(20):201601, 2019.
- [24] Chia-Jui Chou, Bo-Han Lin, Bin Wang, and Yi Yang. Entanglement entropy inequalities in BCFT by holography. *JHEP*, 02:154, 2021.
- [25] Veronika E. Hubeny, Mukund Rangamani, and Massimiliano Rota. The holographic entropy arrangement. *Fortsch. Phys.*, 67(4):1900011, 2019.
- [26] Temple He, Veronika E. Hubeny, and Mukund Rangamani. Superbalance of Holographic Entropy Inequalities. *JHEP*, 07:245, 2020.
- [27] Sergio Hernández-Cuenca, Veronika E. Hubeny, and Hewei Frederic Jia. Holographic entropy inequalities and multipartite entanglement. *JHEP*, 08:238, 2024.